The Canadian Mineralogist
Vol. 33, pp. 349-359 (1995)

SIMS ANALYSIS OF SULFIDE MINERALS FOR Pt AND Au: METHODOLOGY AND RELATIVE SENSITIVITY FACTORS (RSF)

LOUIS J. CABRI

CANMET/Mineral Sciences Laboratories, 555 Booth Street, Ottawa, Ontario K1A 0G1

GREG McMAHON

CANMET/Metals Technology Laboratories, 568 Booth Street, Ottawa, Ontario K1A 0G1

ABSTRACT

Relative sensitivity factors (RSF) were determined for ^{197}Au and ^{198}Pt in some common sulfide minerals using a CAMECA IMS-4f ion microprobe. Sulfides implanted with ^{197}Au and ^{198}Pt were sputtered using a Cs^+ primary beam, and negative secondary ions were measured. Mass interferences were eliminated by operating in a high-mass-resolution mode ($m/\Delta m \approx 2{,}000$), giving rise to average minimum detection-levels ranging from 0.013 to 0.223 ppmw. The RSF values for ^{197}Au are 3.84×10^{18} cm^{-3} ± 9.7% (monoclinic pyrrhotite), 2.67×10^{19} cm^{-3} ± 12.0% (pyrite), 3.69×10^{18} cm^{-3} ± 29.2% (chalcopyrite), and for ^{198}Pt, 1.35×10^{19} cm^{-3} ± 7.4% (chalcopyrite), 1.51×10^{19} cm^{-3} ± 12.3% (monoclinic pyrrhotite), and 9.21×10^{18} cm^{-3} ± 38.1% (pentlandite). In all cases, the reference matrix mass used for the RSF calculations was ^{56}Fe. The higher ^{197}Au RSF values for pyrite, compared to chalcopyrite and pyrrhotite, are attributed, in part, to a larger quantity of electronegative species in pyrite, which tends to inhibit the amount of Au^- emitted.

Keywords: relative sensitivity factors, secondary-ion mass spectrometry, gold, platinum, sulfides, minimum detection-levels.

SOMMAIRE

Nous avons déterminé des facteurs de sensibilité relative pour les isotopes ^{197}Au et ^{198}Pt dans les sulfures courants au moyen d'une microsonde ionique CAMECA IMS-4f. Ces sulfures, dans lesquels ont été implantés les deux isotopes, ont été balayés avec un faisceau d'ions Cs^+ primaires, et la quantité d'ions secondaires négatifs émis a été mesurée. Nous avons pu éliminer les interférences massiques en utilisant le mode de résolution élevée des masses ($m/\Delta m \approx 2{,}000$), ce qui nous a permis d'atteindre un seuil de détection minimum moyen entre 0.013 et 0.223 ppmw. Les valeurs du facteur de sensibilité relative pour l'isotope ^{197}Au sont 3.84×10^{18} cm^{-3} ± 9.7% (pyrrhotite monoclinique), 2.67×10^{19} cm^{-3} ± 12.0% (pyrite), 3.69×10^{18} cm^{-3} ± 29.2% (chalcopyrite), et pour l'isotope ^{198}Pt, 1.35×10^{19} cm^{-3} ± 7.4% (chalcopyrite), 1.51×10^{19} cm^{-3} ± 12.3% (pyrrhotite monoclinique), et 9.21×10^{18} cm^{-3} ± 38.1% (pentlandite). Dans tous les cas, la masse de la matrice de référence utilisée dans les calculs du facteur de sensibilité relative était ^{56}Fe. Les valeurs plus élevées du facteur pour ^{197}Au dans la pyrite, comparée à la chalcopyrite ou la pyrrhotite, seraient dues, en partie, à la plus grande quantité dans la pyrite d'espèces électronégatives, qui ont tendance à atténuer la proportion d'ions Au^- émis.

(Traduit par la Rédaction)

Mots-clés: facteurs de sensibilité relative, spectrométrie de masse des ions secondaires, or, platine, sulfures, seuil de détection.

INTRODUCTION

The use of microbeam analytical techniques for the determination of the concentration of trace elements and their distribution in minerals has increased over the last three decades. Since the arrival of the first generation of electron-probe micro-analyzers, the number and variety of techniques available to the analyst have increased significantly. Today, it is possible to complement data obtained from electron-beam spectroscopies, *e.g.*, electron-probe micro-analysis (EPMA), electron-energy-loss spectroscopy (EELS), with that obtained from proton-beam spectroscopies (particle-induced X-ray excitation, PIXE), gamma-ray spectroscopy (Mössbauer spectroscopy) and ion-beam spectrometries (accelerator mass spectrometry, AMS, and secondary-ion mass spectrometry, SIMS), with each technique having advantages and disadvantages. Of these techniques, SIMS has especially grown in its variety of applications. Minimum limits of detection of less than one part per million by weight (ppmw), depth-profiling capabilities permitting the detection of buried inclusions, the ability to determine isotope abundances, and the possibility of imaging the specimen with any

desired secondary ion to produce maps of element distribution all make SIMS a very attractive and powerful analytical technique to investigate problems in the mineralogical sciences. Reed (1989) has reviewed the application of SIMS in geology, and a large body of literature exists in its application for the determination of trace concentrations of precious metals in various minerals (McIntyre *et al.* 1984, Chryssoulis *et al.* 1986, 1989, Cabri *et al.* 1989, 1991, Chryssoulis & Cabri 1990, Cook & Chryssoulis 1990, Fleet *et al.* 1993, Neumayr *et al.* 1993, Ripley & Chryssoulis 1994, Larocque *et al.* 1995a, b).

Unfortunately, the quantification of SIMS data can be hindered by several complicating factors. These include matrix effects, which refer to differences in sensitivity for a given element in samples of different composition resulting from changes in ionization efficiency and sputtering yield, as well as variations in instrument parameters and ion-collection efficiencies.

In order to account for matrix effects, the use of relative sensitivity factors (RSF) has been adopted for the quantification of SIMS data. The RSF is a multiplying factor used to convert the experimentally measured ion count-rate to atom density, and is unique to the sample matrix, operating conditions and choice of calibrating matrix-mass. It is defined in Equation 1 (Wilson *et al.* 1989, for example), in which the term "impurity" refers to the trace element to be measured:

$$\rho_i = I_i/I_m \cdot RSF \qquad \text{(Eq. 1)}$$

where ρ_i is the density of the impurity atom in atoms cm^{-3}, I_i is the measured count-rate for the impurity secondary ion, and I_m is the measured count-rate for a selected secondary ion from the matrix. The RSF has units of atoms·cm^{-3}, and not only accounts for differences in rates of sputtering, but is also a relative measure of the ionization probability of a given element in a specific matrix.

RSF values may be determined through the use of standards, which can be prepared in two ways. In the first method, a series of standards are prepared by doping the matrix with the element to be measured. Calibration curves relating the counts of the secondary ion of the unknown to a selected species of secondary ion in the matrix are then drawn. McIntyre *et al.* (1984) used this approach to prepare standards of silver- and indium-doped ZnS and PbS in order to determine levels of Ag and In in natural sphalerite and galena. Although applicable in that particular study, this method has several disadvantages. For example, limitations due to solubility and melting temperature may prevent the doping of certain elements in given matrices to the desired levels of concentration. Furthermore, the achievement of a homogeneous distribution of the dopant may prove difficult.

Fortunately, ion implantation can be used to incorporate a known amount of an element into the near-surface region of a sample. Therefore, the production of SIMS standards of almost any element doped into any matrix is possible (Leta & Morrison 1980). In the ion-implantation process, an ion beam of the desired dopant is created, mass-filtered and accelerated to a specified energy toward the matrix to be implanted. Typically, the energy is a few hundred keV, but for heavier masses such as Au and Pt, higher energies are required to obtain a useful distribution with depth. This results in an implantation of the ions into the near-surface region of the specimen. By rastering the implantation beam, a uniform distribution of the dopant in the lateral dimensions is ensured. The current delivered to a selected area of the sample can be measured and used to control the implant fluence. The concentration of the implanted atoms varies with the depth of the implant and typically resembles a Gaussian distribution. The shape of the implant distribution can be monitored to ensure that the implanted species, rather than an interfering mass, is being monitored. Therefore, by comparing the integrated signal of an ion with the total implant fluence, an RSF can be calculated for the implanted species, with respect to a specific matrix, using Equation 2 (Wilson *et al.* 1989, for example):

$$RSF = \phi C I_m t/(d\Sigma I_i - dI_b C) \cdot EM/FC \qquad \text{(Eq. 2)}$$

where ϕ is the implant fluence in atoms cm^{-2}, C is the number of data cycles, I_m is the intensity of the secondary ions in the matrix in counts s^{-1}, t is the duration of the analysis in s $cycle^{-1}$ for the impurity species, d is the crater depth in cm, ΣI_i is the sum of the impurity secondary-ion counts obtained from the depth profile, I_b is the background secondary-ion intensity of I_i in counts $cycle^{-1}$, and EM/FC is the ratio of the counting efficiency of the electron multiplier to that of the Faraday cup.

Although SIMS has been widely used to determine the concentrations of trace amounts of precious metals and platinum-group elements in a number of minerals, RSF values have rarely been reported for ion-implanted standards in minerals, in contrast to semiconducting materials such as Si and GaAs (*e.g.*, Wilson *et al.* 1989, 1994). Chryssoulis *et al.* (1989) derived calibration curves for ^{109}Ag implanted into sphalerite, pyrite, and chalcopyrite. In that study, an O^- primary beam was used with positive secondary ions, and $^{54}Fe^+$ was the matrix mass measured. Similar curves were given for ^{197}Au implanted into pyrite and arsenopyrite by Chryssoulis *et al.* (1989). In these studies, negative secondary ions were detected, and a Cs^+ primary beam was employed. The $^{33}S^-$ signal was used to monitor the secondary ion counts from the matrix. Neumayr *et al.* (1993) listed RSF values for gold implanted into arsenopyrite and löllingite. They used a beam of Cs^+ primary ions, and measured negative secondary ions. The matrix masses measured were S_2^-, $FeAs^-$ and

$FeAsS_2^-$ in arsenopyrite, and $FeAs^-$ and Fe_2As^- in löllingite. Larocque *et al.* (1995b) give RSF values for ^{107}Ag implanted in pyrite using an O_2^+ primary beam and positive secondary ions. The matrix mass measured in this case was $^{57}Fe^{36}S^+$.

It is the purpose of this study to expand the current database of RSF values for precious metals and platinum-group elements in common ore minerals. In particular, new RSF data for ^{197}Au implanted in pyrite, chalcopyrite, and monoclinic pyrrhotite are given, as well as RSF values for ^{198}Pt implanted into monoclinic pyrrhotite, pentlandite, and chalcopyrite.

Experimental Techniques

Implant standards

Minerals used as ion-implantation standards were selected from a variety of sources. Ideally, the minerals should have low concentrations of the element to be implanted, and consist of monomineralic crystalline masses larger than the 1-cm diameter of the implant beam. After selection, the minerals were sectioned and mounted in carbon-loaded 2.5-cm polished sections, which were examined for integrity using optical microscopy. Minerals whose stoichiometry was unknown (*e.g.*, pyrrhotite) or those known to have variable composition (*e.g.*, arsenopyrite, löllingite, pentlandite) were analyzed using EPMA for major and minor elements. Bulk assays were done on a representative quantity of each mineral, and details are documented elsewhere (Cabri, Crocket & Grégoire, in prep.). The minerals used for implant standards in this study are listed in Table 1, together with information on the two standards used by Neumayr *et al.* (1993).

Details of implantation

Implantation of a fluence of 1×10^{13} cm^{-2} ^{198}Pt was carried out in the Department of Physics, University of Western Ontario, using an energy of 1.0 MeV and a current of 2 nA. All implant fluences were determined as areal densities by measuring the total charge accumulated on target through a beam-defining aperture of known area and dividing by the charge of the ion. The isotopic purity of the implants was estimated to be better than 95% (I.V. Mitchell, pers. comm., 18 Dec., 1992). The accuracy of the ^{198}Pt ion-implantation fluences was verified using Rutherford Back-scattering Spectrometry (RBS) on equivalently implanted silicon standards using a 2 MeV $^4He^+$ incident beam. From these experiments, we determined that the implant fluences, including the uniformity, are accurate to within approximately ±5% (W.N. Lennard, pers. comm., 24 Oct., 1994).

Implantation to a fluence of 2.5×10^{13} cm^{-2} ^{197}Au was carried out in the Physical Chemistry Branch, Chalk River Laboratories, AECL Research, at an energy of 1.0 MeV. Fluences were measured by current integration using a 3.5-cm-diameter Faraday cup, which positioned the specimen behind a circular mask 1.2 cm in diameter (*cf.* Chryssoulis *et al.* 1989). The accuracy of the ^{197}Au ion-implantation fluences also was determined using RBS on a series of five implanted silicon standards ranging from 1×10^{14} to 1×10^{15} Au cm^{-2}. The RBS measurements showed the fit between RBS and measured dose of current to be accurate to within about ±5% (J.H. Rolston, pers. comm., 10 July, 1992).

TABLE 1. IMPLANTED SULFIDE STANDARDS

Implant*	Mineral	Source	Locality	EPMA**	Bulk assays (ppb)**
^{197}Au	arsenopyrite	GSC #012826	Santa Eulalia, Mexico	$(Fe_{1.02}Co_{<0.1})As_{0.97}S_{1.01}$	Au: 38
^{197}Au	chalcopyrite	GSC #012532	Grube Friedrichwilhelm, Germany	not done	Au: 40, 40
^{197}Au	löllingite	GSC #016024	Hebron, Maine, USA	$Fe_{1.00}(As_{1.91}S_{0.09})$	Au: 12
^{197}Au	pyrite	GSC #012715	Elba, Italy	not done	Au: 2.3, 5.9
^{197}Au	pyrrhotite	GSC #012616	Santa Eulalia, Mexico	$Fe_{7.04}S_{7.96}$	Au: 45, 52
^{198}Pt	chalcopyrite	CANMET collection	Bruce Mines, Algoma District, Ontario	not done	Pt: < 12
^{198}Pt	pentlandite	Peter Snadjr	Strathcona mine, deep Cu zone (3600L), Ontario	$(Fe_{4.23}Ni_{4.76}Co_{0.05})S_{7.96}$	Pt: 161
^{198}Pt	pyrrhotite	GSC #012616	Santa Eulalia, Mexico	$Fe_{7.04}S_{7.96}$	Pt: 43, 59

*Fluence for ^{197}Au = 2.5×10^{13} atoms/cm^2; for Pt = 1.0×10^{13} atoms/cm^2

**Details of bulk assay methodology and analyses are given in Cabri *et al.* (in prep.)

TABLE 2. SUMMARY OF EXPERIMENTAL PARAMETERS

Primary Ion Beam and Polarity	Cs^+
Secondary Ion Polarity	Negative
Matrix Mass Measured	^{56}Fe
Primary Beam Current	150-550 nA
Primary Beam Accelerating Voltage	10 kV
Impact Energy	14.5 kV
Field Aperture Diameter	750 μm
Contrast Diaphragm Diameter	400 μm
Raster	250 μm
Image Field	150 μm
Diameter of Analysis Area	62 μm

SIMS analyses

All work in the present study was performed using a Cameca IMS-4f double-focusing magnetic sector secondary-ion mass spectrometer. A Cs^+ primary ion beam with an impact energy of 14.5 kV was used, and negative secondary ions were detected. All samples had been previously coated with a thin film of carbon to prevent charging. The experimental parameters are outlined in Table 2.

In order to alleviate the problem of mass interferences associated with the ^{197}Au and ^{198}Pt masses, the mass spectrometer was operated under conditions of high mass-resolution ($m/\Delta m \approx 2000$), which allowed adequate separation of the masses of interest from the undesired interferences. Local calibrations of the magnet were performed using a synthetically prepared $(Fe,Pt)_9S_{10}$ sample with a 0.07 wt% addition of Pt. Mass spectra were acquired from this sample, and the magnet was calibrated on the ^{198}Pt peak. In order to ensure that the calibration was correct, depth profiles were subsequently performed, whereby the masses ^{194}Pt, ^{195}Pt, ^{196}Pt and ^{198}Pt were monitored. By comparing the relative intensities observed and the natural isotopic abundances, it could be quickly determined whether or not the calibration was correct. As experience was gained, the shape of the mass spectrum around the ^{198}Pt peak was easily recognized, and could be used as a fingerprint, thus eliminating the need to acquire the depth profiles.

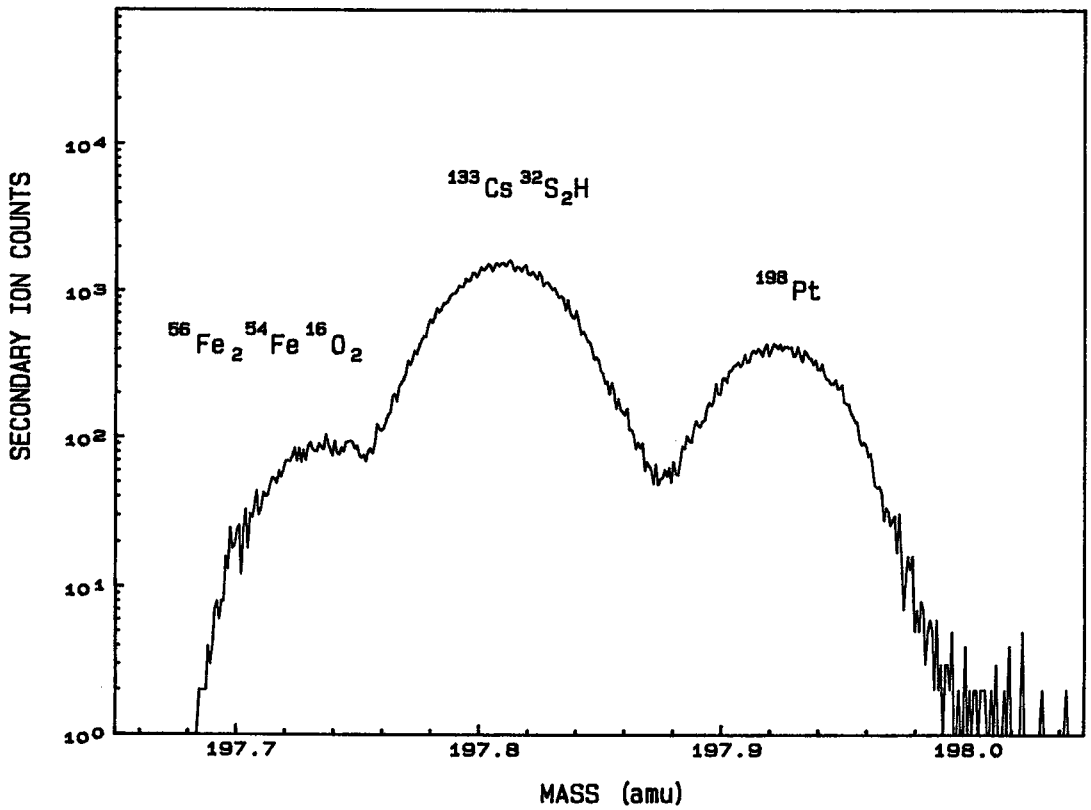

FIG. 1. High-mass-resolution spectrum of synthetic $(Fe,Pt)_9S_{10}$, containing 0.07 wt.% Pt, illustrating the separation of the two interfering masses from that of ^{198}Pt.

Once the magnet had been calibrated correctly, depth profiles were performed on the implanted standards. The mass of interest and a second mass (*e.g.*, $^{56}Fe_2$ + ^{32}S) were recorded, in order to monitor the system's stability and the integrity of the sample, with acquisition times typically 1 s cycle^{-1} for the former and 0.1 s cycle^{-1} for the latter. At the conclusion of the depth profile, the counts for the matrix mass ^{56}Fe were measured on the electron multiplier, which were subsequently used for the RSF calculations. Following the depth profiles, the crater depths were measured using a Tencor Alpha-Step 200 profilometer. Three measurements of depth were taken in each direction across the crater, and an average value was used. The RSF values were then determined using Equation 2 with the SIMS Instrument Control System software, version 4.0, from Charles Evans and Associates.

Results

One of the most useful results of the present study was the identification of the ^{198}Pt fingerprint in the mass spectrum of the synthetic sample. The recognizable pattern allowed a rapid and correct calibration of the magnet. An example of such a mass spectrum is shown in Figure 1, which clearly shows the separation of the ^{198}Pt peak from two interferences, calculated to be $^{133}Cs^{32}S_2H$ and $^{56}Fe_2{}^{54}Fe^{16}O_2$. Once this triplet of peaks in the mass spectrum was identified, it was a straightforward process to calibrate the magnet on the ^{198}Pt peak. The fingerprint in the ^{197}Au region of the spectra of sulfide minerals studied included two lower mass-interferences, calculated to be $^{54}Fe_2{}^{57}Fe^{32}S$ and $^{133}Cs^{32}S_2$. A similar mass-spectrum fingerprint has been given for ^{197}Au in arsenopyrite (Cabri &

TABLE 3. RSF VALUES CALCULATED FOR ^{56}Fe MATRIX AND MINIMUM DETECTION LIMITS FOR ^{197}Au IMPLANTED IN PYRITE

Session	RSF (cm^{-3})	MDL (ppmw)	Sputter Rate (Å/s)	Beam Current (nA)	^{56}Fe Matrix Counts
1	$2.88x10^{19}$	0.170	11.0	166.8	$1.51x10^5$
1	$3.17x10^{19}$	0.244	11.2	170.5	$1.63x10^5$
1	$2.89x10^{19}$	0.199	9.99	151.6	$1.40x10^5$
1	$2.84x10^{19}$	0.164	9.98	149.4	$1.39x10^5$
2	$2.95x10^{19}$	0.086	9.73	150.6	$1.48x10^5$
2	$3.54x10^{19}$	0.284	9.63	140.1	$1.42x10^5$
2	$2.89x10^{19}$	0.173	11.1	160.4	$1.68x10^5$
2	$2.83x10^{19}$	0.103	11.3	158.6	$1.78x10^5$
2	$2.75x10^{19}$	0.177	11.3	159.7	$1.76x10^5$
2	$2.82x10^{19}$	0.201	11.5	164.0	$1.81x10^5$
3	$2.52x10^{19}$	0.267	9.91	147.5	$3.71x10^5$
3	$2.51x10^{19}$	0.222	9.81	150.1	$2.92x10^5$
3	$2.94x10^{19}$	0.347	10.3	157.3	$3.56x10^5$
3	$3.17x10^{19}$	0.253	10.2	154.2	$3.72x10^5$
3	$3.06x10^{19}$	0.281	10.3	154.7	$3.64x10^5$
4	$2.44x10^{19}$	0.346	10.7	157.1	$3.13x10^5$
4	$2.70x10^{19}$	0.282	10.7	157.8	$3.42x10^5$
5	$8.55x10^{18}$	0.217	28.5	374.7	$2.28x10^5$
5	$1.00x10^{19}$	0.222	27.1	361.7	$2.55x10^5$

Mean RSF value for 19 analyses $\bar{x} = 2.67x10^{19}$ cm^{-3}
$s = 8.51x10^{18}$ (standard deviation for RSF values with population parameter taken as n-1)

Student t-variable with n-1 degrees of freedom at 95% confidence levels $t_{95\%} = 2.080$
$\bar{x} \pm t_{n-1}\ s/\sqrt{n} = 2.67x10^{19} \pm 3.21x10^{18}$
$= 2.67x10^{19} \pm 12.0\%$

Mean MDL $\bar{x} = 0.223$

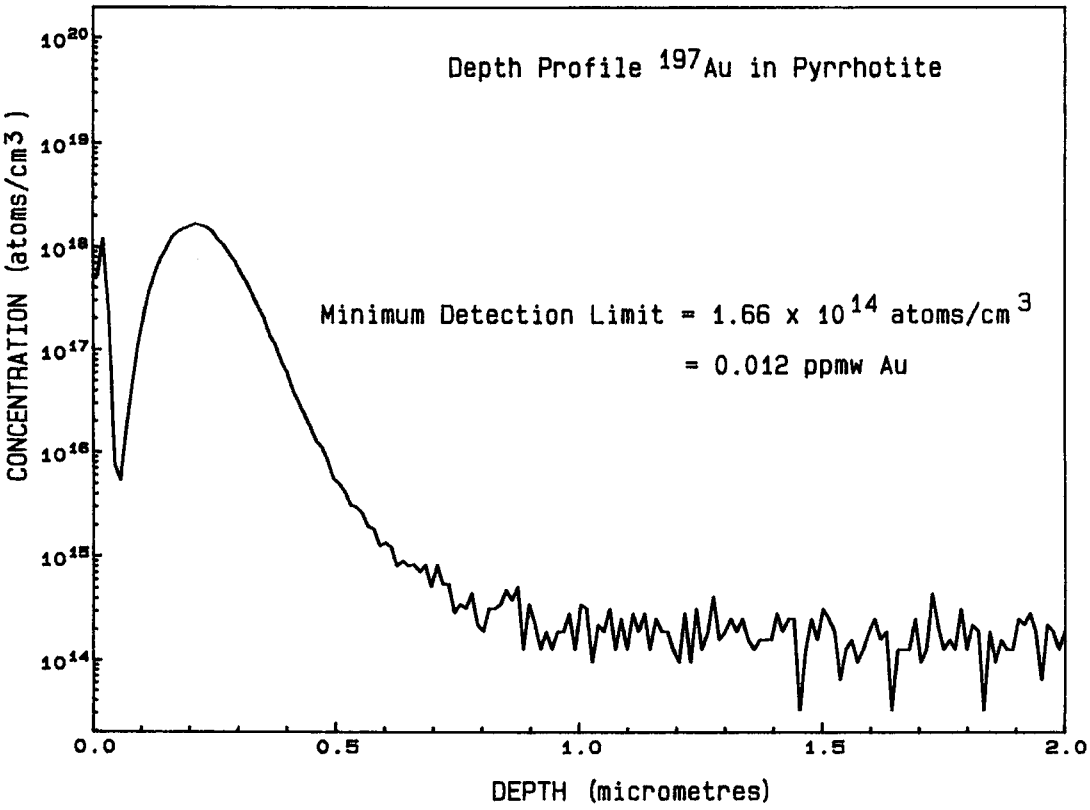

FIG. 2. Typical depth-profile for ^{197}Au implanted in pyrrhotite. The initial high count-rate is attributed to sputtering through the carbon coating.

TABLE 4. RSF VALUES CALCULATED FOR ^{56}Fe MATRIX AND MINIMUM DETECTION LIMITS FOR ^{197}Au IMPLANTED IN PYRRHOTITE

Session	RSF (cm^{-3})	MDL (ppmw)	Sputter Rate (Å/s)	Beam Current (nA)	^{56}Fe Matrix Counts
1	4.36×10^{18}	0.078	41.2	357	1.23×10^{5}
2	3.98×10^{18}	0.019	39.0	409	1.33×10^{5}
2	4.44×10^{18}	0.012	37.4	372	1.39×10^{5}
2	4.07×10^{18}	0.021	37.0	368	1.35×10^{5}
3	3.53×10^{18}	0.054	35.3	411	2.11×10^{5}
3	3.47×10^{18}	0.094	34.9	410	2.11×10^{5}
3	3.64×10^{18}	0.115	34.9	408	2.17×10^{5}
3	3.28×10^{18}	0.129	34.2	408	2.19×10^{5}

Mean RSF value for 8 analyses $\bar{x} = 3.84\times10^{18}$ cm^{-3}
$s = 4.43\times10^{17}$

$t_{95\%} = 2.365$
$\bar{x} \pm t_{n-1}\ s/\sqrt{n} = 3.84\times10^{18} \pm 3.71\times10^{17}$
$= 3.84\times10^{18} \pm 9.7\%$

Mean MDL $\bar{x} = 0.065$

TABLE 5. RSF VALUES CALCULATED FOR ^{56}Fe MATRIX AND MINIMUM DETECTION LIMITS FOR ^{197}Au IMPLANTED IN CHALCOPYRITE

Session	RSF (cm^{-3})	MDL (ppmw)	Sputter Rate (Å/s)	Beam Current (nA)	^{56}Fe Matrix Counts
1	$5.39x10^{18}$	0.062	38.0	397	$2.16x10^{5}$
1	$5.70x10^{18}$	0.054	37.5	386	$2.22x10^{5}$
2	$2.99x10^{18}$	0.159	35.6	409	$2.52x10^{5}$
2	$2.94x10^{18}$	0.187	35.7	407	$2.44x10^{5}$
2	$3.11x10^{18}$	0.178	28.9	405	$2.52x10^{5}$
2	$3.04x10^{18}$	0.166	36.2	406	$2.56x10^{5}$
2	$2.51x10^{18}$	0.118	35.0	391	$2.89x10^{5}$
2	$2.54x10^{18}$	0.118	36.0	391	$2.91x10^{5}$

Mean RSF value for 8 analyses $\bar{x} = 3.69x10^{18}$ cm^{-3}
$s = 1.29x10^{18}$

$t_{95\%} = 2.365$
$\bar{x} \pm t_{n-1}\ s/\sqrt{n} = 3.69x10^{18} \pm 1.10x10^{18}$
$= 3.69x10^{18} \pm 29.2\%$

Mean MDL $\bar{x} = 0.130$

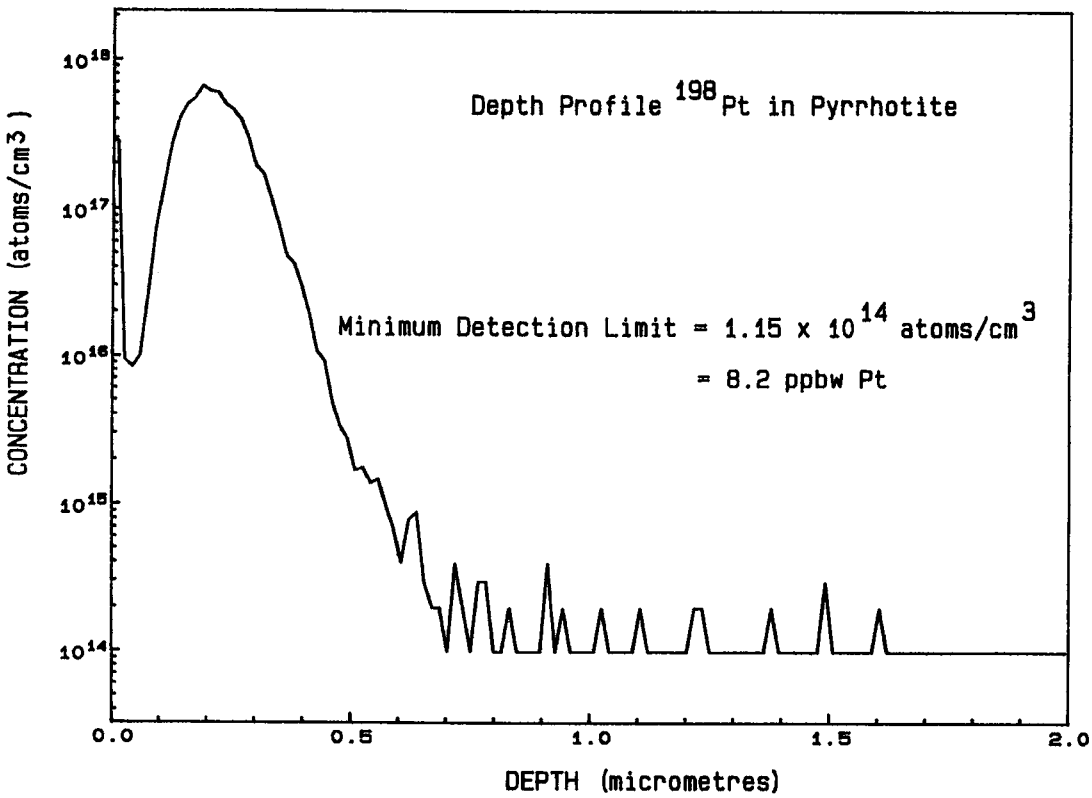

FIG. 3. Typical depth-profile for ^{198}Pt implanted in pyrrhotite.

TABLE 6. RSF VALUES CALCULATED FOR ^{56}Fe MATRIX AND MINIMUM DETECTION LIMITS FOR ^{198}Pt IMPLANTED IN PENTLANDITE

Session	RSF (cm^{-3})	MDL (ppmw)	Sputter Rate (Å/s)	Beam Current (nA)	^{56}Fe Matrix Counts
1	$1.24x10^{19}$	0.065	59.0	390	$6.65x10^{4}$
1	$1.39x10^{19}$	0.033	58.9	381	$7.68x10^{4}$
2	$5.07x10^{18}$	0.018	55.1	403	$7.42x10^{4}$
2	$8.21x10^{18}$	0.013	51.0	406	$1.21x10^{5}$
2	$7.01x10^{18}$	0.013	49.8	411	$1.09x10^{5}$
2	$8.61x10^{18}$	0.013	49.8	408	$1.30x10^{5}$

Mean RSF value for 6 analyses $\bar{x} = 9.21x10^{18}$ cm^{-3}
$s = 3.35x10^{18}$

$t_{95\%} = 2.571$; $\bar{x} \pm t_{n-1}\ s/\sqrt{n} = 9.21x10^{18} \pm 3.51x10^{18}$
$= 9.21x10^{18} \pm 38\%$

Mean MDL $\bar{x} = 0.026$

TABLE 7. RSF VALUES CALCULATED FOR ^{56}Fe MATRIX AND MINIMUM DETECTION LIMITS FOR ^{198}Pt IMPLANTED IN PYRRHOTITE

Session	RSF (cm^{-3})	MDL (ppmw)	Sputter Rate (Å/s)	Beam Current (nA)	^{56}Fe Matrix Counts
1	$1.75X10^{19}$	0.001	42.6	427	$3.09x10^{5}$
1	$1.94x10^{19}$	0.011	42.1	418	$3.30x10^{5}$
1	$1.82x10^{19}$	0.012	34.6	381	$2.86x10^{5}$
1	$1.80x10^{19}$	0.012	37.3	354	$2.82x10^{5}$
2	$1.25x10^{19}$	0.013	47.6	417	$2.77x10^{5}$
2	$1.29x10^{19}$	0.009	47.7	415	$2.92x10^{5}$
3	$1.60x10^{19}$	0.111	34.6	359	$1.27x10^{5}$
3	$1.31x10^{19}$	0.022	33.5	288	$1.12x10^{5}$
3	$1.18x10^{19}$	0.013	40.0	414	$1.83x10^{5}$
3	$1.14x10^{19}$	0.012	39.9	409	$1.66x10^{5}$
4	$1.45x10^{19}$	0.014	32.9	419	$1.98x10^{5}$
4	$2.55x10^{19}$	0.020	22.1	423	$2.27x10^{5}$
4	$1.13x10^{19}$	0.010	48.8	420	$2.20x10^{5}$
4	$1.48x10^{19}$	0.008	42.3	422	$2.99x10^{5}$
4	$1.54x10^{19}$	0.009	42.8	442	$3.13x10^{5}$
4	$1.59x10^{19}$	0.008	42.6	437	$3.22x10^{5}$
5	$1.61x10^{19}$	0.014	43.6	453	$3.15x10^{5}$
5	$1.44x10^{19}$	0.018	43.1	447	$2.89x10^{5}$
6	$1.65x10^{19}$	0.028	48.6	411	$1.18x10^{5}$
6	$2.65x10^{18}$	0.028	45.1	411	$1.65x10^{5}$
6	$1.65x10^{19}$	0.029	50.9	397	$1.06x10^{5}$
6	$1.66x10^{19}$	0.036	49.9	393	$9.78x10^{4}$

Mean RSF value for 22 analyses $\bar{x} = 1.51x10^{19}$ cm^{-3}
$s = 4.19x10^{18}$

$t_{95\%} = 2.080$
$\bar{x} \pm t_{n-1}\ s/\sqrt{n} = 1.51x10^{19} \pm 1.86x10^{18}$
$= 1.51x10^{19} \pm 12.3\%$

Mean MDL $\bar{x} = 0.020$

TABLE 8. RSF VALUES CALCULATED FOR ^{56}Fe MATRIX AND MINIMUM DETECTION LIMITS FOR ^{198}Pt IMPLANTED IN CHALCOPYRITE

Session	RSF (cm^{-3})	MDL (ppmw)	Sputter Rate (Å/s)	Beam Current (nA)	^{56}Fe Matrix Counts
1	$1.54X10^{19}$	0.013	50.5	417	$5.79x10^5$
1	$1.50x10^{19}$	0.011	50.8	418	$5.92x10^5$
2	$1.18x10^{19}$	0.014	40.0	414	$1.83x10^5$
2	$1.14x10^{19}$	0.013	39.9	409	$1.66x10^5$
2	$8.49x10^{18}$	0.012	41.1	449	$1.92x10^5$
2	$1.22x10^{19}$	0.011	41.5	463	$2.78x10^5$
3	$1.50x10^{19}$	0.009	41.1	444	$4.34x10^5$
3	$1.52x10^{19}$	0.008	44.4	446	$4.85x10^5$
4	$1.50x10^{19}$	0.010	52.2	455	$5.38x10^5$
4	$1.29x10^{19}$	0.009	51.9	451	$4.92x10^5$
4	$1.43x10^{19}$	0.011	46.7	453	$4.86x10^5$
4	$1.38x10^{19}$	0.010	45.6	449	$4.65x10^5$
5	$1.46x10^{19}$	0.017	63.6	533	$1.97x10^5$
5	$1.31x10^{19}$	0.020	51.1	402	$1.60x10^5$
5	$1.54x10^{19}$	0.018	50.6	398	$1.78x10^5$
5	$1.00x10^{19}$	0.016	75.1	395	$1.55x10^5$
5	$1.54x10^{19}$	0.020	53.8	402	$1.67x10^5$
5	$1.31x10^{19}$	0.020	54.9	395	$1.50x10^5$

Mean RSF value for 18 analyses $\bar{x} = 1.35x10^{19}$ cm^{-3}
$s = 2.01x10^{18}$

$t_{95\%} = 2.110$; $\bar{x} \pm t_{n-1}\ s/\sqrt{n} = 1.35x10^{19} \pm 1.00x10^{18}$
$= 1.35x10^{19} \pm 7.4\%$

Mean MDL $\bar{x} = 0.013$

Chryssoulis 1990, Chryssoulis 1990).

The results of the RSF calculations for ^{197}Au implanted in pyrite are presented in Table 3, and a typical depth-profile is shown in Figure 2. The error calculations for this and all subsequent sets of data are given at the 95% confidence level assuming a normal distribution of data points. The minimum detection-limit, in parts per million by weight, is given for each depth-profile, with an average value of 0.242 × 20.2% ppmw Au being calculated for the entire set of samples. Similarly, an average RSF value of 2.67×10^{19} cm^{-3} ± 12.0% was also calculated for the entire set of data. The sputter rate and beam current are also given in Table 3. The ratio of sputter rate to beam current is a useful parameter to cross-check the validity of the profilometer measurements; it was found to be constant for both within and between sessions. The fact that the ratios are all similar strongly suggests that the data acquired over the five different sessions are comparable. In a similar manner, the RSF values for ^{197}Au implanted in pyrrhotite and chalcopyrite are summarized in Tables 4 and 5, respectively. The depth profiles for these minerals are similar to that for pyrite (Fig. 2).

The RSF values for ^{198}Pt implanted in pentlandite, pyrrhotite, and chalcopyrite are summarized in Tables 6, 7, and 8, respectively. A typical depth-profile from this set of data is shown in Figure 3.

Discussion

The RSF values and minimum limits of detection of Au and Pt in the various sulfide minerals studied are shown in Table 9. The variation in reproducibility is due to subtle differences in experimental conditions

TABLE 9. SUMMARY OF ^{197}Au AND ^{198}Pt RSF VALUES AND MIMINUM DETECTION LIMITS FOR SULFIDE MINERALS STUDIED

	Chalcopyrite	Pyrrhotite	Pentlandite	Pyrite
^{197}Au RSF	$3.69x10^{18}\pm29.2\%$	$3.84x10^{18}\pm9.7\%$	-	$2.67x10^{19}\pm12.0\%$
^{198}Pt RSF	$1.35x10^{19}\pm7.4\%$	$1.51x10^{19}\pm12.3\%$	$9.21x10^{18}\pm38.1\%$	-
^{197}Au MDL	$0.130\pm32.8\%$	$0.065\pm59.2\%$	-	$0.223\pm15.2\%$
^{198}Pt MDL	$0.013\pm15.3\%$	$0.020\pm50.0\%$	$0.026\pm84.8\%$	-

Note: RSF in cm^{-3} calculated for ^{56}Fe matrix, and MDL in ppmw

between sessions. The RSF values for ^{197}Au and ^{198}Pt vary within about ±15% for most of the implant standards, except for ^{197}Au in chalcopyrite and ^{198}Pt in pentlandite. The reason(s) for poorer reproducibility in the latter two examples is not readily apparent, but may be related to imperfections in these particular standards. These imperfections may be a poor polished surface, or the presence of fine inclusions of another mineral, such as pyrrhotite. The fact that fewer experimental runs were performed on these samples also contributes to larger uncertainties in the RSF values. However, as mentioned above, instrumental conditions for individual sessions play a role in the determination of RSF values. For example, the ^{197}Au RSF is 2.847×10^{18} cm^{-3} ± 9.6% for chalcopyrite in session 2, may be compared with the value from all sessions of 3.69×10^{18} cm^{-3} ± 29.2%.

Part of the contribution to the background of a SIMS depth profile is the inherent precious-metal bulk concentration in the chosen sulfide mineral. This is used to estimate the minimum detection-limit (MDL). As can be seen from Table 1, these backgrounds range from about 2 to 161 ppbw. Greater recorded counts for the background must be attributed to experimental conditions during a particular analytical session, such as accumulated contamination on the immersion lens and cover plate (memory effects), which can occur as a result of previous analyses of Au- or Pt-coated specimens, or specimens rich in Au or Pt. Ions originating from the crater walls also increase the MDL for an ion-implanted sample. Experimentally obtained background-levels below (as well as above) those determined by bulk analyses may be due to inhomogeneous distribution of these trace metals in the sulfides. In any case, it is essential to determine the MDL for each analytical session that involves analyses of minerals, especially those with compositions below one ppmw.

Table 9 contains an interesting result for the ^{197}Au RSF values: they are about one order of magnitude lower for chalcopyrite and pyrrhotite compared to pyrite. Considering the chemical similarities of the matrices involved, it is interesting to speculate why this behavior occurs. Recognizing that the emission of secondary ions is sensitive to the presence of electropositive or electronegative species at the sample's sputtered surface, an important trend in the mineral matrices is observed. Pyrite (66.6 at.% S) has more of the strongly electronegative S species than pyrrhotite (53.3 at.% S) or chalcopyrite (50 at.% S). The presence of a larger quantity of electronegative species in the sample may reduce the likelihood that sputtered Au can retain an extra electron and be emitted as Au^-. A calculation of the ratio of the peak secondary Au ion counts to the peak Au concentration normalized to the beam current showed this to be true. For pyrite, the average value over all the experiments was calculated to be 5.67×10^{-17} ± 20.9% (in units of counts cm^3 $atoms^{-1}$ nA^{-1}), whereas for pyrrhotite and chalcopyrite, average values of 7.81×10^{-17} ± 7.45% and 1.13×10^{-16} ± 15.6% were calculated, respectively. This phenomenon may also explain why the ^{198}Pt RSF values do not vary that much in chalcopyrite, pyrrhotite and pentlandite (47 at.% S).

ACKNOWLEDGEMENTS

We are grateful to H. Gary Ansell, Geological Survey of Canada, for providing a large number of the minerals used in this study, and to Peter Snadjr, Falconbridge, for a pentlandite sample. We also acknowledge the help of the following at CANMET: J.H. Gilles Laflamme performed the EPMA, M. Beaulne and J. Greer made the polished sections, V. Chartrand helped with the ion microprobe, and Dr. J.A. Jackman provided helpful comments and discussions on an earlier draft and on the revised manuscript. In addition, we thank the following for comments and suggestions: Editor R.F. Martin, Dr. R.G. Wilson, and a second, anonymous, referee.

REFERENCES

CABRI, L.J. & CHRYSSOULIS, S.L. (1990): Advanced methods of trace-element microbeam analyses. *In* Advanced Microscopic Studies of Ore Minerals (J.L. Jambor & D.J. Vaughan, eds.). *Mineral. Assoc. Can., Short-Course Handbook* **17**, 341-377.

———, ———, CAMPBELL, J.L. & TEESDALE, W.J. (1991): Comparison of in-situ gold analyses in arsenian pyrite. *J. Appl. Geochem.* **6**, 225-230.

———, ———, DE VILLIERS, J.P.R., LAFLAMME, J.H.G. & BUSECK, P.R. (1989): The nature of "invisible" gold in arsenopyrite. *Can. Mineral.* **27**, 353-362.

CHRYSSOULIS, S.L. (1990): Quantitative trace metal analysis of sulfide and sulfarsenide minerals by SIMS. *In* Proc. Secondary Ion Mass Spectroscopy, SIMS VII (A. Benninghoven, C.A. Evans, K.D. McKeegan, H.A. Storms & H.W. Werner, eds.). John Wiley & Sons, Chichester, U.K. (405-408).

——— & CABRI, L.J. (1990): The significance of gold mineralogical balances in mineral processing. *Inst. Mining Metall. Trans.* **99**, C1-C10.

———, ——— & LENNARD, W. (1989): Calibration of the ion microprobe for quantitative trace precious metal analyses of ore minerals. *Econ. Geol.* **84**, 1684-1689.

———, CHAUVIN, W.J. & SURGES, L.J. (1986): Trace element analysis by secondary ion mass spectrometry with particular reference to silver in the Brunswick sphalerite. *Can. Metall. Quart.* **25**, 233-239.

COOK, N.J. & CHRYSSOULIS, S.L. (1990): Concentrations of "invisible gold" in the common sulfides. *Can. Mineral.* **28**, 1-16.

FLEET, M.E., CHRYSSOULIS, S.L., MACLEAN, P.J., DAVIDSON, R. & WEISENER, C.G. (1993): Arsenian pyrite from gold deposits: Au and As distribution investigated by SIMS and EMP, and colour staining and surface oxidation by XPS and LIMS. *Can. Mineral.* **31**, 1-17.

LAROCQUE, A.C.L., HODGSON, C.J., CABRI, L.J. & JACKMAN, J.A. (1995a): Ion-microprobe analysis of pyrite, chalcopyrite and pyrrhotite from the Mobrun VMS deposit in northwestern Quebec: evidence for metamorphic remobilization of Au. *Can. Mineral.* **33**, 373-388.

———, JACKMAN, J.A., CABRI, L.J. & HODGSON, C.J. (1995b): Calibration of the ion microprobe for the determination of silver in pyrite and chalcopyrite from the Mobrun VMS deposit, Rouyn–Noranda, Quebec. *Can. Mineral.* **33**, 361-372.

LETA, D.P. & MORRISON, G.H. (1980): Ion implantation for in-situ quantitative ion microprobe analysis. *Anal. Chem.* **52**, 277-280.

MCINTYRE, N.S., CABRI, L.J., CHAUVIN, W.J. & LAFLAMME, J.H.G. (1984): Secondary ion mass spectrometric study of disolved silver and indium in sulfide minerals. *Scanning Electron Microsc.* **III**, 1139-1146.

NEUMAYR, P., CABRI, L.J., GROVES, D.I., MIKUCKI, E.J. & JACKMAN, J.A. (1993): The mineralogical distribution of gold and relative timing of gold mineralization in two Archean settings of high metamorphic grade in Australia. *Can. Mineral.* **31**, 711-725.

REED, S.J.B. (1989): Ion microprobe analysis – a review of geological applications. *Mineral. Mag.* **53**, 3-24.

RIPLEY, E.M. & CHRYSSOULIS, S.L. (1994): Ion microprobe analysis of platinum-group elements in sulfide and arsenide minerals from the Babbitt Cu–Ni deposit, Duluth complex, Minnesota. *Econ. Geol.* **89**, 201-210.

WILSON, R.G., STEVIE, F.A., CHRYSSOULIS, S.L. & IRWIN, R.B. (1994): Secondary ion mass spectrometry relative sensitivity factors for Ru, Rh, Pr, Eu, Tm, Lu, Re, Os, and Ir. *J. Vac. Sci. Technol.* **A12**, 2415-2419.

———, ——— & MAGEE, C.W. (1989): *Secondary Ion Mass Spectrometry – A Practical Handbook for Depth Profiling and Bulk Impurity Analysis*. John Wiley & Sons, New York, N.Y.

Received November 2, 1994, revised manuscript accepted February 3, 1995.